

Magnetic excitations and anomalous spin-wave broadening in multiferroic FeV₂O₄Qiang Zhang,^{1,2,*} Mehmet Ramazanoglu,^{1,2} Songxue Chi,³ Yong Liu,¹ Thomas A. Lograsso,^{1,4} and David Vaknin^{1,2,†}¹Ames Laboratory, Ames, Iowa 50011, USA²Department of Physics and Astronomy, Iowa State University, Ames, Iowa 50011, USA³Oak Ridge National Laboratory, Oak Ridge, Tennessee 37831, USA⁴Division of Materials Sciences and Engineering, Iowa State University, Ames, Iowa 50011, USA

(Received 21 April 2014; revised manuscript received 3 June 2014; published 25 June 2014)

We report on the different roles of two orbital-active Fe²⁺ at the *A* site and V³⁺ at the *B* site in the magnetic excitations and on the anomalous spin-wave broadening in FeV₂O₄. FeV₂O₄ exhibits three structural transitions and successive paramagnetic (PM)–collinear ferrimagnetic (CFI)–noncollinear ferrimagnetic (NCFI)/ferroelectric transitions. The high-temperature tetragonal/PM–orthorhombic/CFI transition is accompanied by the appearance of a large energy gap in the magnetic excitations due to strong spin-orbit-coupling-induced anisotropy at the Fe²⁺ site. While there is no measurable increase in the energy gap from the orbital ordering of V³⁺ at the orthorhombic/CFI–tetragonal/NCFI transition, anomalous spin-wave broadening is observed in the orthorhombic/CFI state due to V³⁺ spin fluctuations at the *B* site. The spin-wave broadening is also observed at the zone boundary without softening in the NCFI/ferroelectric phase, which is discussed in terms of magnon-phonon coupling. Our study also indicates that the Fe²⁺ spins without the frustration at the *A* site may not play an important role in inducing ferroelectricity in the tetragonal/NCFI phase of FeV₂O₄.

DOI: 10.1103/PhysRevB.89.224416

PACS number(s): 75.85.+t, 61.05.fg, 75.25.–j, 75.47.Lx

I. INTRODUCTION

Understanding the orbital degrees of freedom and their coupling with spin and lattice degrees of freedom has emerged as a forefront topic in modern condensed-matter physics as these coupled degrees of freedom play a central role in inducing various novel phenomena [1]. Vanadium spinel oxides with formula AV₂O₄ [2] are ideal systems to study the orbital ordering (OO) by virtue of the fact that the 3*d*² high-spin configuration of V³⁺ is accommodated in the triply degenerate *t*_{2*g*} states rendering it with orbital degrees of freedom. For a nonmagnetic occupancy of the *A* site by a divalent ion such as Zn, Mg, and Cd [3], there is usually a structural transition from cubic to tetragonal, followed by a magnetic ordering at a lower temperature. Replacing *A* by a magnetic ion Mn²⁺ in a 3*d*⁵ high-spin configuration without orbital degrees of freedom leads to successive paramagnetic (PM)–collinear ferrimagnetic (CFI)–noncollinear ferrimagnetic (NCFI) magnetic transitions [4], while the latter one is accompanied by a similar cubic-tetragonal structural transition. In FeV₂O₄, the *A*-site Fe²⁺ with a high-spin 3*d*⁶ configuration and three electrons in the doubly degenerate *e* states gives rise to orbital degrees of freedom [5,6]. FeV₂O₄ exhibits similar PM-CFI-NCFI magnetic transitions as in MnV₂O₄, but the competition or cooperation between two orbital-active Fe²⁺ and V³⁺ leads to three structural transitions, and a fourth one, albeit controversial [5,7,8]. Previous investigations have focused on the orbital ordering of V³⁺ at the *B* site and its effect on the cubic-tetragonal transition and the magnetic excitations in AV₂O₄ (*A* = Zn, Mg, Cd, and Mn) [9–12]. However, the effect of the orbital ordering at the *A* site on the magnetic excitations in vanadium spinel oxides is not clear yet. FeV₂O₄

provides a good candidate to investigate the roles of orbital orderings not only on the *B* site, but also on the *A* site.

Distinct from perovskite oxides, relatively few spinel oxides such as CdV₂O₄ [13], ACr₂O₄ [14,15] (*A* = Co or Fe), were reported so far to display multiferroicity in the spinel oxide family. The reasons why the spinel oxides do not favor multiferroicity are still not clear. Recently, Zhang *et al.* discovered multiferroicity in FeV₂O₄ [7], where the ferroelectricity is not found in the collinear ferrimagnetic phase but only emerges in the noncollinear ferrimagnetic phase. It is of interest to compare the spin dynamics [16] in these two distinct magnetic phases, and also to figure out the source of the spin frustration in FeV₂O₄ since spin frustration is usually related to the appearance of the ferroelectricity in various noncollinear magnetic phases [17,18]. Motivated by the above issues, we studied high-quality FeV₂O₄ single crystal using a combination of magnetization measurements, and elastic and inelastic neutron-scattering techniques.

II. EXPERIMENTAL DETAILS

The FeV₂O₄ crystal was grown using the floating zone method. The dc susceptibility measurements were carried out on a Magnetic Property Measurement System (Quantum Design, SQUID). A big piece of crystal of the mass ≈1 g was cut for the elastic and inelastic neutron-scattering measurements that were conducted on the HB3 spectrometer (located at the High Flux Isotope Reactor at Oak Ridge National Laboratory, USA) with a fixed final energy (*E* = 14.7 meV).

III. RESULTS AND DISCUSSION

Figure 1(a) shows the splitting of the *q* scans of the (400) structural Bragg peak in the cubic setting at several representative temperatures. The schematic pictures of distortion of the crystals and the definition of directions of crystalline axes

*qzhangemail@gmail.com

†vaknin@ameslab.gov

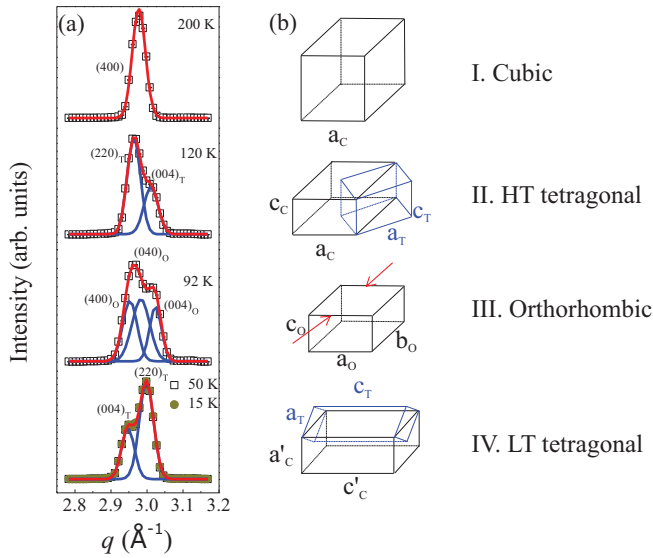


FIG. 1. (Color online) (a) Splitting of the (400) peak in the cubic setting of FeV_2O_4 at representative temperatures. Symbols are experimental data; red lines are the sum of two/three Gaussian fits; blue lines are the single Gaussian fit. (b) Schematic pictures of the distortion of the crystals and the definition of directions of crystalline axes in different phases. Note that in both HT and LT tetragonal phases, the unit cell in the tetragonal setting is one-half of the unit cell distorted from the cubic unit cell above T_S .

using different settings in different structures are summarized in Fig. 1(b). At 120 K, one (400) peak splits to $(220)_T$ and $(400)_T$ in the tetragonal notation, suggesting the c axis of the cubic unit cell is compressed due to Jahn-Teller distortion of FeO_4 [5,7,8] driven by a ferroic $\text{Fe}^{2+} 3z^2-r^2$ OO [19] and the cubic structure transforms into a high-temperature (HT) tetragonal structure with $c_c < a_c$ (a_c is the lattice constant in the cubic phase). As temperature further decreases to 92 K, one of the a axes in the HT tetragonal phase is compressed [5], resulting in a structural transition to orthorhombic phase, which can be seen from the splitting of two peaks to three peaks $(400)_O$, $(040)_O$, and $(004)_O$. At 50 K, these three peaks evolve back to two peaks, indicating another structural transition to a low-temperature (LT) tetragonal phase. As opposed to the HT tetragonal phase, the peak position q of $(004)_T$ is smaller than that of the $(220)_T$ peak in the LT tetragonal phase. Moreover, the peak intensity of the low- q peak is weaker than that of the high- q peak in the LT tetragonal phase. Thus, the LT tetragonal phase with $c > a$ is different from the HT tetragonal phase with $c < a$ and the tetragonal c axes in these two tetragonal phases are perpendicular to each other in one unit cell. This indicates that the compressed axis (b_O or a_O) in the orthorhombic phase, becomes equal to the c_O , and therefore, the orthorhombic phase evolves to a LT tetragonal phase and the third axis becomes the new c axis in the tetragonal setting. Based on the above discussion, we notice that during the structural transformation from a HT tetragonal phase to a LT tetragonal phase in FeV_2O_4 , the orthorhombic phase cannot be avoided. It should be noted that as shown in Fig. 1(a), no change is observed in the q scans of the (400) structural Bragg peak between 50 and 15 K,

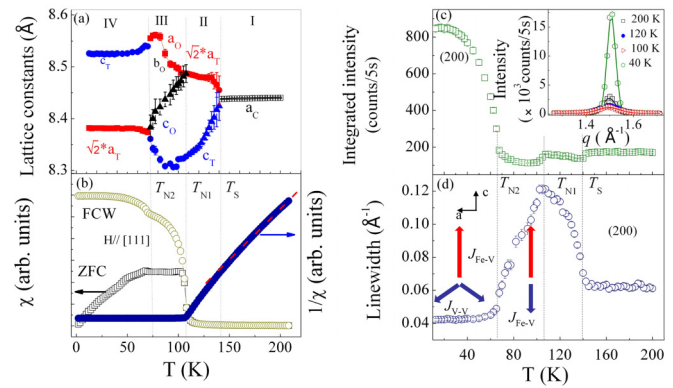


FIG. 2. (Color online) (a) Temperature dependence of the lattice parameters in FeV_2O_4 . (b) Temperature dependence of the dc susceptibility (squares) after zero-field cooled and field cooled with $H \parallel [111]$ axis in FeV_2O_4 . The solid circles show the inverse susceptibility. Temperature dependence of (c) the integrated intensity and (d) the linewidth of the (200) peak. The inset of (c) shows representative q scans of the (200) peak. The solid lines are fits to a Gaussian function. The schematic magnetic structures projected on the ac plane with the main magnetic interactions below/above T_{N2} are also shown in (d). The long arrows and short arrows represent Fe^{2+} and V^{3+} spins, respectively. The dashed lines mark the three transitions.

excluding any structural transition at around 35 K as reported by Katsufuji *et al.* [5] but not by others [8,19].

The obtained lattice constants as a function of temperature shown in Fig. 2(a) indicate that there are three structural transitions: cubic-high-temperature (HT) tetragonal ($c < a$) at $T_S = 140$ K, HT tetragonal-orthorhombic at $T_{N1} = 110$ K, and orthorhombic-LT tetragonal at $T_{N2} = 70$ K. It is worthwhile noting that T_{N2} here, consistent with the value in Ref. [5], is a little higher than 56 K in polycrystalline samples [7,8], and 60 K [8] or 65 K [19] in single crystal form, reflecting strong suppression of the nonstoichiometry, i.e., $x \approx 0$ in the formulation $(\text{Fe}^{2+})(\text{Fe}_x^{3+}\text{V}_{2-x}^{3+})\text{O}_4$ in our crystal as a lower value of x causes an increase of T_{N2} [20]. Thus, the investigation on the stoichiometric FeV_2O_4 crystal can minimize the effect of nonstoichiometry and reveal intrinsic magnetic excitations.

Figure 2(b) shows the temperature dependence of the dc susceptibility with zero-field cooling (ZFC) and field-cooled warming (FCW) modes in a magnetic field of 1000 Oe parallel to the [111]. Below T_{N1} , a rapid increase in the susceptibility is ascribed to the PM to CFI ordering where the Fe^{2+} moments are parallel to the [001] and the V^{3+} moments are antiparallel to the Fe^{2+} moments via antiferromagnetic (AFM) coupling $J_{\text{Fe-V}}$ [7,8]. Another jump in the FC susceptibility below T_{N2} results from CFI to NCFI transition due to the V^{3+} canting [7,8] along any of the $\langle 111 \rangle$ directions [8]. The schematic CFI and NCFI magnetic structures projected on the ac plane with the main magnetic interactions [7,8] are shown in Fig. 2(d). The inverse susceptibility shows a deviation below T_S , indicating a magnetoelastic coupling [5] at T_S . We note that FeCr_2O_4 with only orbital-active Fe^{2+} exhibits similar PM cubic-PM tetragonal ($c < a$)-CFI orthorhombic transitions [21] without the lowest one at T_{N2} . Thus, the two transitions at T_S and

T_{N1} in FeV_2O_4 are mainly ascribed to the involvement of orbital-active Fe^{2+} [19]. The LT tetragonal phase with $c > a$ in FeV_2O_4 is unique in all the vanadium spinel oxides, suggesting both orbital-active Fe^{2+} and V^{3+} are necessary [5] to induce the third structural transition at T_{N2} .

Figures 2(c) and 2(d) show the temperature dependence of integrated intensity and peak linewidth of the high-symmetry-forbidden (200) reflection in FeV_2O_4 . The peak is present at all measured temperatures and exhibits anomalies at the three transitions. We note that the observed (200) is not due to $\lambda/2$ leakage as the PG filters remove this higher-order wavelength to better than one part in 3×10^6 as measured on the nuclear (220) Bragg peak and the forbidden (110) at 200 K. The observed (200) peak above T_S at 200 K has a pure structural origin due to anisotropy of the local environment around the transition-metal atoms with no contribution from charge ordering or OO, as discussed in other spinels, such as $A\text{Fe}_2\text{O}_4$ ($A = \text{Mn}, \text{Co}, \text{and Fe}$) [22]. Whereas weak anomalies at T_S and T_{N1} in the intensities and linewidths are present, the (200) reflection with higher intensity and sharper peak below T_{N2} is mainly magnetic in origin, which confirms the occurrence of V^{3+} spin canting as depicted in Fig. 2(d).

Constant- \mathbf{Q} energy scans were measured at the zone center (220) at various temperatures and at various \mathbf{Q} 's along $[\text{H H } 0]$ at CFI (90 K) and NCFI (3.5 K) phases. As shown in Fig. 3(a), a clear energy gap ≈ 8 meV at (220) in the low- E region is observed at 3.5 K and the gap drops smoothly with increasing temperature. In the damped simple harmonic oscillator approximation [23–25], the neutron-scattering cross section is given by

$$\frac{d^2\sigma}{d\Omega dE}(\mathbf{q}, E) \propto \frac{A_q \Gamma E}{\{E^2 - [E_0(\mathbf{q})]^2 + \Gamma^2 E^2\} (1 - e^{-E/kT})^{-1}}, \quad (1)$$

where A_q is q -dependent intensity, Γ is the spin-wave damping factor and can also characterize the intrinsic magnon width,

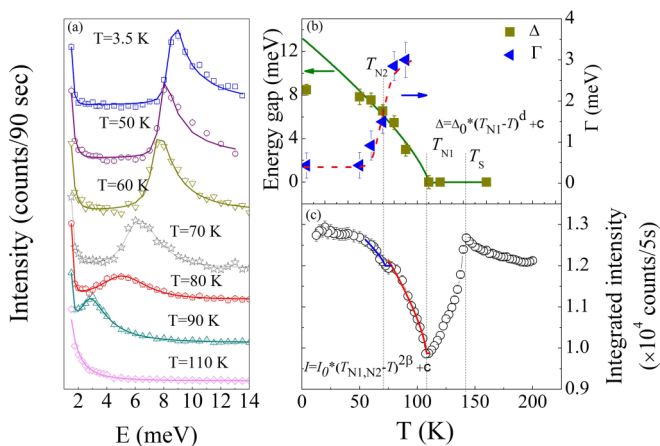


FIG. 3. (Color online) (a) Constant- \mathbf{Q} energy scans measured at the zone center (220) at various temperatures. The solid lines are fits using the model described in the text. (b) Temperature dependence of (b) the energy gap, damping factor Γ , and (c) the integrated intensity of the (220) Bragg peak. The solid lines are fits to the data (see text for more details).

and $(1 - e^{-E/kT})^{-1}$ is the Bose factor. In the small- \mathbf{q} limit, the spin waves around (220) zone center can be approximately described by an anisotropic linear dispersion relation [4,23]:

$$E_0(\mathbf{q}) = \sqrt{\Delta^2 + v_{ab}^2(q_x^2 + q_y^2)}, \quad (2)$$

where v is the spin-wave velocity and Δ is the energy gap. The constant- \mathbf{Q} energy scans have been fitted using Eqs. (1) and (2) after convolution with the instrumental resolution using the RESLIB program [26].

The temperature dependence of the energy gap at (220) zone center is shown in Fig. 3(b). Compared with the behavior of the energy gap in MnV_2O_4 [4] where only V has orbital degrees of freedom, FeV_2O_4 shows three main differences: (1) In FeV_2O_4 the gap emerges below T_{N1} , whereas for MnV_2O_4 it only emerges below T_{N2} ($=53$ K). (2) The gap in FeV_2O_4 is much higher. (3) No obvious increase in the energy gap (≈ 1.5 meV) as observed in MnV_2O_4 is found in FeV_2O_4 below T_{N2} .

In the temperature range $T_{N2} < T < T_{N1}$ for both MnV_2O_4 and FeV_2O_4 , the magnetic structures are similar without OO of V^{3+} [19]. The main difference in this temperature region between these two systems is that Fe^{2+} is orbital ordered whereas Mn^{2+} is not. Thus, the appearance of an energy gap below T_{N1} in FeV_2O_4 is due to the involvement of Fe^{2+} OO and not related to V^{3+} ions. It has been shown that the sole PM-CFI magnetic transition without any OO cannot induce an energy gap below T_{N1} in MnV_2O_4 [4]. Furthermore, the sole ferroic $\text{Fe}^{2+} 3z^2-r^2$ OO [19] does not induce the energy gap below T_{N1} since the OO is formed at a higher temperature T_S . Therefore, the spin-orbit-coupling-induced anisotropy at the A-site Fe^{2+} is responsible for the appearance of the gap. High-resolution synchrotron x-ray measurements on FeV_2O_4 [19] have shown that there is a strong spin-orbit coupling at the A-site Fe^{2+} and the CFI ordering below T_{N1} triggers the structural transition to orthorhombic with a lower symmetry via the spin-orbit coupling, similar to $A\text{Cr}_2\text{O}_4$ ($A = \text{Fe}$ and Cu) with only an orbital-active ion at the A site [21]. Compared with MnV_2O_4 , the much higher energy gap in FeV_2O_4 results from stronger spin-orbit coupling at the Fe^{2+} A site than that of the V^{3+} B site in MnV_2O_4 . The larger ordered moment of $4.0\mu_B$ [8] of Fe^{2+} below T_{N1} than that of the V ion ($1.3\mu_B$) in MnV_2O_4 [4] also contributes to the higher gap. Below T_{N2} , although spin ordering of V^{3+} is similar and V^{3+} becomes orbital ordered in both MnV_2O_4 and FeV_2O_4 , the absence of a measurable increase in energy gap below T_{N2} in FeV_2O_4 implies nearly quenched orbital moments or a very weak SO coupling for the V^{3+} , consistent with soft x-ray magnetic circular dichroism experiments [27] and theoretical calculations [6].

To get further insight into the temperature evolution of the energy gap, we performed a least-square fit using power law $\Delta(T) \propto (T_{N1} - T)^d$ and obtained an exponent $d \approx 0.75$ below T_{N1} , similar to the value of ≈ 0.73 in MnV_2O_4 below T_{N2} [4]. This indicates the the energy gap induced by the anisotropy at the Fe^{2+} site in FeV_2O_4 has similar temperature evolution and critical behavior as the energy gap due to the anisotropy at the V^{3+} B site in MnV_2O_4 . We also modeled the temperature dependence of the integrated intensity of Bragg peak (220) around T_{N1} and T_{N2} using $I(T) \propto (T_{N1,N2} - T)^{2\beta}$, yielding critical exponents $\beta_1 \approx 0.353$ at T_{N1} and $\beta_2 \approx 0.381$ at T_{N2} .

This indicates that FeV_2O_4 is close to the three-dimensional (3D) Heisenberg ($\beta = 0.36$) or 3D Ising ($\beta = 0.33$) models. These two critical exponents are similar to the values near T_{N1} and T_{N2} reported in MnV_2O_4 [4]. The comparison of β_1 with d values below T_{N1} in FeV_2O_4 indicates that the temperature dependence of the energy gap varies like the square of the staggered magnetization [4] once the CFI ordering sets in.

We emphasize that the spin-wave damping factor Γ [see Fig. 3(b)] increases rapidly at T_{N2} . We also used the Lorentz function convoluted with the spectrometer resolution function to model constant- \mathbf{Q} energy scans yielding FWHM values very close to Γ . Raising the temperature usually leads to a gradual spin-wave broadening but the clear anomaly at T_{N2} excludes thermal effect only. We argue that the spin-wave broadening in $T_{N2} < T < T_{N1}$ originates from strong fluctuations of V^{3+} spins on the B site in the CFI phase prior to their true canting below T_{N2} . Such spin fluctuations of V^{3+} affect the Fe spin waves and therefore lead to the anomalous spin-wave broadening in $T_{N2} < T < T_{N1}$.

Representative constant- \mathbf{Q} E scans at various \mathbf{Q} 's along the $[\text{H H 0}]$ in the NCFI/ferroelectric phase are shown in Fig. 4(a). The solid lines are the best fit using the model described above and the obtained spin-wave dispersions at the two different magnetic states are shown in Fig. 4(b). Similar to the behavior at the (220) zone center, Γ at each fixed \mathbf{Q} at 90 K is significantly larger than that at 3.5 K, as shown in the inset of Fig. 4(c). Compared with the spin-wave spectra of MnV_2O_4 [4,28], the symmetric lowest-energy spin wave should be the acoustic mode due to the oscillations of Fe spins. Further measurements on other spin-wave branches, especially four branches of V spin waves [28] at higher energies, are necessary to obtain accurate magnetic interactions such as $J_{\text{Fe-V}}$, in-plane $J_{\text{V-V}}$, out-of-plane $J_{\text{V-V}}$, $J_{\text{Fe-Fe}}$, and the single-ion anisotropies. Note that the spin-wave shapes at 90 and 3.5 K are very similar with only a shift of ≈ 5 meV indicating that Fe^{2+} spins are not influenced obviously below T_{N2} . This suggests that there is no significant spin frustration at the Fe^{2+} site in the NCFI/ferroelectric phase, consistent with powder neutron diffraction results that show the direction of the Fe^{2+} spins remains along the c axis below/above T_{N2} . Therefore, the Fe spins without magnetic frustration at the A site are not mainly responsible for the appearance of the ferroelectricity below T_{N2} . Instead, the competition between the AFM $J_{\text{V-V}}$ and AFM $J_{\text{Fe-V}}$ induces strong spin frustration at the V site resulting in the canting of V^{3+} spins, which plays a major role in the appearance of the ferroelectricity based on (extended) spin-current models [7,14,29].

As shown in Fig. 4(b), the spin waves in FeV_2O_4 exhibit a significant broadening but without softening at the zone boundary. $\Gamma \approx 0.7$ meV for $H \leq 2.2$, but shows a significant increase/step to ≈ 3 meV above $H \approx 2.4$. In Fig. 4(c), the average Γ/E ratio ≈ 0.11 is much smaller than that of the metallic ferromagnetic $\text{La}_{2-2x}\text{Sr}_{1+2x}\text{Mn}_2\text{O}_7$ with $\Gamma/E \approx 0.33-0.46$ [30], consistent with the high insulating behavior of FeV_2O_4 [7]. Furthermore, the $\Gamma/E \approx 0.07$ at the zone center and ≈ 0.14 at the zone boundary exhibit weak q sensitivity of Γ/E and Γ is not linear with respect to E . All these features exclude magnon-electron scattering [30] as the main mechanism for spin-wave broadening. Theoretical calculations [31] have shown that magnon-phonon coupling

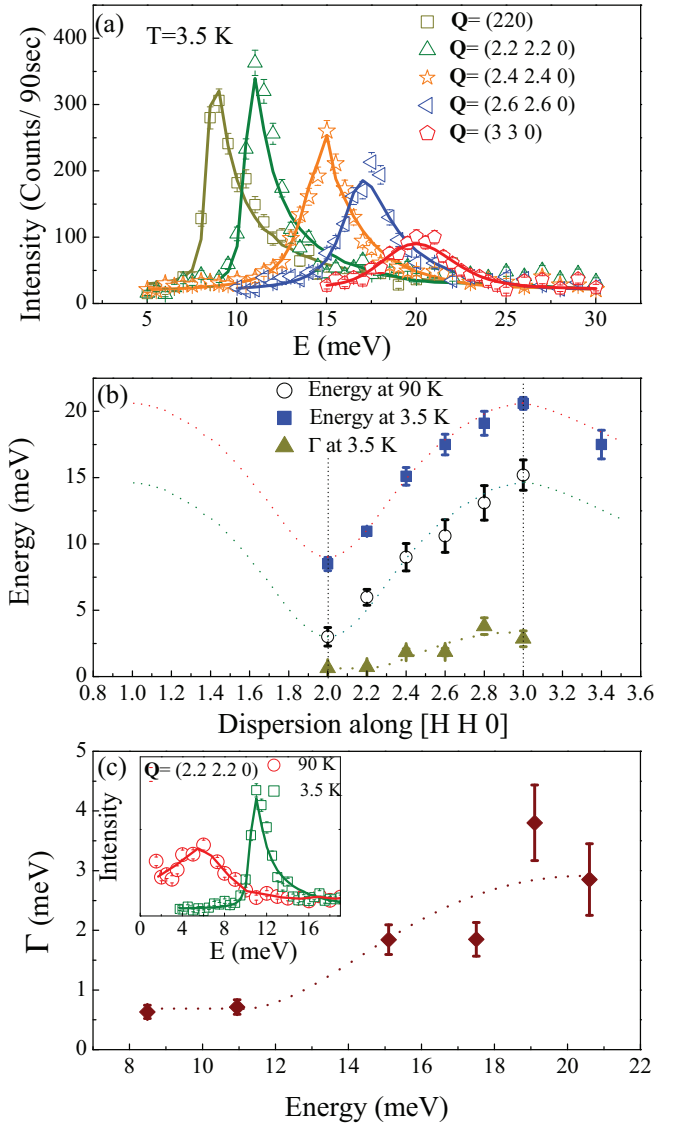


FIG. 4. (Color online) (a) Constant- \mathbf{Q} E scans at different \mathbf{Q} 's along $[\text{H H 0}]$ at 3.5 K in FeV_2O_4 . (b) Low-energy Fe spin waves with dispersion along $[\text{H H 0}]$ at 90 and 3.5 K, and the wave-vector dependence of spin-wave damping Γ at 3.5 K. (c) Energy dependence of Γ at 3.5 K. The dotted lines are guides to the eye. The inset shows a comparison of the raw data at $\mathbf{Q} = (2.2 2.2 0)$ at 90 and 3.5 K.

can increase the spin-wave damping without softening the dispersion. Dai *et al.* [32] reported a significant spin-wave broadening at the zone boundary with a step in Γ in a few manganese perovskites and demonstrated the role of magnon-phonon coupling as a mechanism of such anomalous broadening. The existence of a strong coupling between spin, orbital, and lattice degrees of freedom [7] and the step in Γ in FeV_2O_4 imply that magnon-phonon coupling plays the main role in the spin-wave broadening without softening at the zone boundary.

IV. CONCLUSION

In summary, neutron-scattering studies on FeV_2O_4 crystal reveal the different roles of two orbital-active Fe^{2+} at the A site

and V^{3+} at the B site in the magnetic excitations. The strong spin-orbit coupling at the Fe^{2+} A site induces a significant energy gap below T_{N1} with little contribution from the V^{3+} . The absence of a change in energy gap below T_{N2} is evidence for a very weak SO coupling or significantly quenched orbital moment of the V^{3+} . The important role of orbital-active Fe^{2+} at the A site on the magnetic excitations is expected to be applicable to other spinels with orbital-active ions at that site, such as ACr_2O_4 ($A = Fe^{2+}$ or Cu^{2+}).

Comparing the Fe spin waves below and above T_{N2} precludes significant spin frustration at the Fe^{2+} site, indicating Fe^{2+} may not play an important role in inducing ferroelectricity and the ferroelectricity mainly results from the canting V spins with strong frustration at the B site. The anomalous spin-wave broadening is observed in the collinear ferrimagnetic phase indicative of possible V^{3+} spin fluctuations prior to

their true canting in the noncollinear ferrimagnetic phase. The spin-wave broadening also exists at the zone boundary without obvious spin-wave softening due to magnon-phonon coupling.

ACKNOWLEDGMENTS

Research at Ames Laboratory is supported by the U.S. Department of Energy, Office of Basic Energy Sciences, Division of Materials Sciences and Engineering under Contract No. DE-AC02-07CH11358. Use of the high flux isotope reactor at the Oak Ridge National Laboratory was supported by the U.S. Department of Energy, Office of Science, Office of Basic Energy Sciences, under Contract No. DE-AC02-06CH11357.

-
- [1] Y. Tokura and N. Nagaosa, *Science* **288**, 462 (2000).
- [2] P. G. Radaelli, *New J. Phys.* **7**, 53 (2005).
- [3] S. Nizioł, *Phys. Status Solidi A* **18**, K11 (1973).
- [4] V. O. Garlea, R. Jin, D. Mandrus, B. Roessli, Q. Huang, M. Miller, A. J. Schultz, and S. E. Nagler, *Phys. Rev. Lett.* **100**, 066404 (2008).
- [5] T. Katsufuji, T. Suzuki, H. Takei, M. Shingu, K. Kato, K. Osaka, M. Takata, H. Sagayama, and T. Arima, *J. Phys. Soc. Jpn.* **77**, 053708 (2008).
- [6] S. Sarkar and T. Saha-Dasgupta, *Phys. Rev. B* **84**, 235112 (2011).
- [7] Q. Zhang, K. Singh, F. Guillou, C. Simon, Y. Breard, V. Caignaert, and V. Hardy, *Phys. Rev. B* **85**, 054405 (2012).
- [8] G. J. MacDougall, V. O. Garlea, A. A. Aczel, H. D. Zhou, and S. E. Nagler, *Phys. Rev. B* **86**, 060414(R) (2012).
- [9] N. B. Perkins and O. Sikora, *Phys. Rev. B* **76**, 214434 (2007), and references therein.
- [10] S. Di Matteo, G. Jackeli, and N. B. Perkins, *Phys. Rev. B* **72**, 020408(R) (2005).
- [11] H. Tsunetsugu and Y. Motome, *Phys. Rev. B* **68**, 060405(R) (2003).
- [12] R. Nanguneri and S. Y. Savrasov, *Phys. Rev. B* **86**, 085138 (2012).
- [13] G. Giovannetti, A. Stroppa, S. Picozzi, D. Baldomir, V. Pardo, S. Blanco-Canosa, F. Rivadulla, S. Jodlauk, D. Niermann, J. Rohrkamp, T. Lorenz, S. Streltsov, D. I. Khomskii, and J. Hemberger, *Phys. Rev. B* **83**, 060402(R) (2011).
- [14] H. Katsura, N. Nagaosa, and A. V. Balatsky, *Phys. Rev. Lett.* **95**, 057205 (2005).
- [15] K. Singh, A. Maignan, C. Simon, and C. Martin, *Appl. Phys. Lett.* **99**, 172903 (2011).
- [16] J. W. Lynn, *J. Supercond. Novel Magn.* **13**, 263 (2000).
- [17] Taka-hisa Arima, *J. Phys. Soc. Jpn.* **80**, 052001 (2011).
- [18] J.-H. Kim, M. A. van der Vegte, A. Scaramucci, S. Artyukhin, J.-H. Chung, S. Park, S.-W. Cheong, M. Mostovoy, and S.-H. Lee, *Phys. Rev. Lett.* **107**, 097401 (2011).
- [19] Y. Nii, H. Sagayama, T. Arima, S. Aoyagi, R. Sakai, S. Maki, E. Nishibori, H. Sawa, K. Sugimoto, H. Ohsumi, and M. Takata, *Phys. Rev. B* **86**, 125142 (2012).
- [20] N. Liu, K. H. Zhao, X. L. Shi, and L. W. Zhang, *J. Appl. Phys.* **111**, 124112 (2012).
- [21] S. Bordács, D. Varjas, I. Kézsmárki, G. Mihály, L. Baldassarre, A. Abouelsayed, C. A. Kuntscher, K. Ohgushi, and Y. Tokura, *Phys. Rev. Lett.* **103**, 077205 (2009).
- [22] G. Subías, J. Garcia, M. G. Proietti, J. Blasco, H. Renevier, J. L. Hodeau, and M. C. Sánchez, *Phys. Rev. B* **70**, 155105 (2004).
- [23] M. Ramazanoglu, J. Lamsal, G. S. Tucker, J.-Q. Yan, S. Calder, T. Guidi, T. Perring, R. W. McCallum, T. A. Lograsso, A. Kreyssig, A. I. Goldman, and R. J. McQueeney, *Phys. Rev. B* **87**, 140509 (2013).
- [24] D. K. Pratt, A. Kreyssig, S. Nandi, N. Ni, A. Thaler, M. D. Lumsden, W. Tian, J. L. Zarestky, S. L. Bud'ko, P. C. Canfield, A. I. Goldman, and R. J. McQueeney, *Phys. Rev. B* **81**, 140510(R) (2010).
- [25] F. Ye, P. Dai, J. A. Fernandez-Baca, D. T. Adroja, T. G. Perring, Y. Tomioka, and Y. Tokura, *Phys. Rev. B* **75**, 144408 (2007).
- [26] A. Zheludev, www.neutron.ethz.ch/research/resources/reslib.
- [27] J.-S. Kang, J. Hwang, D. H. Kim, E. Lee, W. C. Kim, C. S. Kim, S. Kwon, S. Lee, J.-Y. Kim, T. Ueno, M. Sawada, B. Kim, B. H. Kim, and B. I. Min, *Phys. Rev. B* **85**, 165136 (2012).
- [28] J.-H. Chung, J.-H. Kim, S.-H. Lee, T. J. Sato, T. Suzuki, M. Katsumura, and T. Katsufuji, *Phys. Rev. B* **77**, 054412 (2008).
- [29] T. A. Kaplan and S. D. Mahanti, *Phys. Rev. B* **83**, 174432 (2011).
- [30] T. G. Perring, D. T. Adroja, G. Chaboussant, G. Aeppli, T. Kimura, and Y. Tokura, *Phys. Rev. Lett.* **87**, 217201 (2001).
- [31] N. Furukawa, *J. Phys. Soc. Jpn.* **68**, 2522 (1999).
- [32] P. Dai, H. Y. Hwang, J. Zhang, J. A. Fernandez-Baca, S.-W. Cheong, C. Kloc, Y. Tomioka, and Y. Tokura, *Phys. Rev. B* **61**, 9553 (2000).